The Cryosphere Discuss., 9, 5817–5847, 2015
www.the-cryosphere-discuss.net/9/5817/2015/
doi:10.5194/tcd-9-5817-2015

The Cryosphere Discussions
Open Access

Small-scale disturbances in the stratigraphy of the NEEM ice core: observations and numerical model simulations

D. Jansen[1], M.-G. Llorens[2,1], J. Westhoff[2], F. Steinbach[2,1], S. Kipfstuhl[1], P. D. Bons[2], A. Griera[3], and I. Weikusat[1,2]

[1]Alfred Wegener Institute Helmholtz Centre for Polar and Marine Research, Bremerhaven, Germany
[2]Department of Geosciences, Eberhard Karls University Tübingen, Tübingen, Germany
[3]Departament de Geologia, Universitat Autò noma de Barcelona, Cerdanyola del V., Spain

Received: 29 July 2015 – Accepted: 1 October 2015 – Published: 29 October 2015

Correspondence to: D. Jansen (daniela.jansen@awi.de)

Published by Copernicus Publications on behalf of the European Geosciences Union.

Small-scale disturbances in the stratigraphy of the NEEM ice core

D. Jansen et al.

Abstract

Disturbances on the centimetre scale in the stratigraphy of the NEEM ice core (North Greenland) can be mapped by an optical line scanner as long as the ice does have a visual layering, such as, for example, cloudy bands. Different focal depths allow, to a certain extent, a three dimensional view of the structures. In this study we present a detailed analysis of the visible folds, discuss their characteristics and frequency and present examples of typical fold structures. We also analyse the structures with regard to the deformation boundary conditions under which they formed. The structures evolve from gentle waves at about 1500 m to overturned z-folds with increasing depth. Occasionally, the folding causes significant thickening of layers. Their similar-fold shape indicates that they are passive features and are probably not initiated by rheology differences between alternating layers. Layering is heavily disturbed and tracing of single layers is no longer possible below a depth of 2160 m. c-axes orientation distributions for the corresponding core sections were analysed where available in addition to visual stratigraphy. The data show axial-plane parallel strings of grains with c-axis orientations that deviate from that of the matrix, which shows a single-maximum fabric at the depth where the folding occurs.

Numerical modelling of crystal viscoplasticity deformation and dynamic recrystallisation was used to improve the understanding of the formation of the observed structures during deformation. The modelling reproduces the development of bands of grains with a tilted orientation relative to the single maximum fabric of the matrix, and also the associated local deformation. We conclude from these results that the observed folding is a consequence of localized deformation at the boundaries of kink bands.

1 Introduction

The NEEM (North Greenland Eemian Ice drilling) ice core, located at 77°27′ N 51°3.6′ W in the northwest of Greenland, has been drilled between June 2008 and

TCD
9, 5817–5847, 2015

July 2012. It is located on a topographic ridge, which dips towards the northwest so that the surface velocities on the ice divide have a non-negligible component of along ridge flow of about 6 m a^{-1} (NEEM community members, 2013). In July 2010 the bedrock was reached at 2537.36 m depth. The site has been chosen in order to recover an undisturbed Eem warm-period ice layer. However, it was found later that the ice below 2200 m was heavily disturbed and probably folded on a large scale (NEEM community members, 2013).

Visual stratigraphy of the NEEM ice core revealed folding also on a small scale, with fold amplitudes varying from less than 1 cm to a few decimetres (Samyn et al., 2011). These types of folds occur well above the large scale disturbances reported by the NEEM community members (2013). Similar structures have been found in the lower parts of other deep ice cores (Alley et al., 1997; Thorsteinsson, 1996; Svensson et al., 2005; Faria et al., 2010; Fitzpatrick et al., 2014). Stratigraphy bands are visualized by an indirect light source scattering on surfaces inside the ice, mainly particles and air bubbles/hydrates (Svensson et al., 2005). High impurity content is found in ice that originates from snow accumulated during glacial periods. Changing impurity contents between ice from glacial and interglacial periods have been linked to rheological differences (e.g. Paterson, 1991) and may lead to deformation heterogeneities, such as non-uniform thinning.

Due to their potential influence on the integrity of the climatic record, folds have been subject to modelling studies (e.g. Waddington et al., 2001). Thorsteinsson and Waddington (2002) explored the amplification of small disturbances in the layering of ice cores for isotropic and anisotropic conditions, investigating the potential for the existence of overturned folds near ice sheet centres. Azuma and Goto-Azuma (1996) concluded from model studies with an anisotropic flow law that an inclined single maximum fabric could lead to vertical strain even in simple shear and thus influence the stratigraphy. They also suggested that horizontal variations in the inclinations could then cause alternating thickening and thinning of layers, leading to folding or boudinage in the stratigraphy. However, the initial formation of the disturbances is not fully understood.

Here we present a characterisation of the small-scale folding observed in the NEEM ice core. Another feature occasionally observed along with folding in deep ice cores are "fabric stripes" (Alley et al., 1997). They describe bands of deviating grain orientations with respect to the surrounding matrix, which is essentially a single maximum fabric in regions where folding occurs. We discuss possible folding mechanisms and the link to the so called "Alley-stripes" in the crystal fabric of grains. Microstructural modelling with ELLE reproduces similar fabrics and fold structures to the ones we observe in the NEEM ice core.

2 Methods

The data used in this study were obtained by different observational methods, which will be introduced only briefly in the following section. For technical details we recommend to check the original literature cited in the subsections.

2.1 Linescan visual stratigraphy

The visual stratigraphy of the NEEM ice core was recorded by means of an automated linescan instrument (see Svensson et al., 2005 for a detailed description of the instrument and data from the North GRIP ice core). Clear ice appears dark when illuminated by an indirect light source. Dust particles or bubbles cause scatter of light and make the ice appear bright in the linescan image. A clear correlation between backscatter and dust content has been found in the North Grip ice core (Svensson et al., 2005). The method can be applied directly in the field and in the case of the NEEM ice core was applied continuously for the entire core, with a gap between 860 and 1150 m, which corresponds to the brittle zone where the core quality did not allow preparation for the linescanner. For the NEEM ice core the linescan images were recorded with a standardised exposure time and three focal planes within the ice core section with a vertical distance of 1 cm (Kipfstuhl, 2010). This allows to a certain degree a three-dimensional mapping of the visible layering in the ice core. The data are stored in high-resolution (118 pixel cm^{-1}) bmp images. One drawback of this method is, of course, that it only shows disturbances in the ice if scattering surfaces are included. However, it is possible to even reveal structures at low dust content by means of image processing and filtering.

2.2 Automated Fabric Analyzer

The crystal fabric orientation of discrete samples was measured using a G50 Automatic Fabric Analyzer (Australian *Russell-Head* type, see e.g. Russell-Head and Wilson, 2001; Peternell et al., 2010, data set: Weikusat and Kipfstuhl, 2010). Samples cut from the physical properties part of the NEEM core were cut to 250 µm thin sections to measure c-axis crystal lattice orientations by polarized light microscopy, where the thin section is placed between systematically varying crossed polarizers (e.g. Wilson and Russell-Head, 2003). The data coverage is much better than in previous ice cores with continuous sampling of selected core sections (bags) to investigate meter-scale variations in fabric throughout the core. However, due to the time-consuming preparation of the samples it was not possible to produce a continuous record.

2.3 Microstructural modelling with ELLE and full field crystal plasticity

We use 2-D numerical modelling to investigate the development of strain localization in a polycrystalline aggregate during simple shear deformation. The simulation approach couples a full field method based on the fast Fourier transform (FFT) that simulates viscoplastic deformation, with two front-tracking codes that simulate dynamic recrystallisation processes (DRX), both included within the open-source numerical modelling platform ELLE (http://www.elle.ws; Bons et al., 2008). ELLE has been successfully used to simulate evolution of microstructures during deformation, such as

TCD
9, 5817–5847, 2015
Small-scale disturbances in the stratigraphy of the NEEM ice core
D. Jansen et al.

recrystallization (Piazolo et al., 2008; Roessiger et al., 2011, 2014) or strain localisation (Jessell et al., 2005; Griera et al., 2011, 2013). The full-field crystal plasticity (FFT) code (Lebensohn, 2001; Lebensohn et al., 2008; Montagnat et al., 2014a) simulates deformation by pure viscoplastic dislocation glide. An experimental run consists of iterative applications of small increments ($\Delta\gamma = 0.04$) of simple shear deformation, each followed by a sub-loop of processes simulating dynamic recrystallisation (grain boundary migration and recovery). While grain boundary migration covers the motion of high-angle grain boundaries, recovery achieves decrease in intracrystalline heterogeneities by means of local rotation without motion of high-angle boundaries. The recrystallisation sub-loop may be called more than once to simulate the different balance between deformation and recrystallisation as a function of strain rate, since all simulations are performed with the same intrinsic mobility value (M_0) and boundary-diffusion activation energy (Q) (Roessiger et al., 2014; Llorens et al., 2015).

Exchange of data between ELLE and FFT is possible, as both use periodic boundary conditions and the physical space is discretised into a shared regular node mesh.

The ELLE data structure consists of three layers: (1) a network of nodes (boundary nodes or *bnodes*) that are connected by straight boundary segments that define the high-angle grain boundaries that enclose individual ice grains, (2) a set of unconnected nodes (*unodes*) to map lattice orientations and dislocation densities, used for the FFT calculation, and (3) a passive marker grid utilised to track finite strain. Distances between nodes are kept between 5.5×10^{-3} and 2.5×10^{-3} times the unit distance (in a 1×1 bounding box), by removing *bnodes* when their neighbours are too close or adding *bnodes* when two nodes are too far apart. The space is discretised in a mesh of 256×256 Fourier points, resulting in a unit cell defined by 65 536 discrete nodes. Each *unode* represents a small area or crystallite with a certain lattice orientation, defined by Euler angles, and a dislocation density value. The ELLE data structure has fully wrapping boundaries. The 10 cm × 10 cm initial microstructure has 1632 grains, each with a homogeneous lattice orientation, showing a c-axis preferred orientation almost perpendicular to the shear plane, in order to simulate an intrinsic anisotropic material.

TCD
9, 5817–5847, 2015

The misorientation between grains was set at < 5° (i.e. initial noise). Dislocation glide of ice-single crystal was defined by slip on the basal {0001} {11-20}, prismatic {1-100} {11-20} and pyramidal systems {11-22} {11-23}. In these simulations, the ratio A of critical resolved shear stress (CRSS) for non-basal vs. basal slip systems was set to $A = 20$. The same stress exponent ($n = 3$) is set for all slip systems. The physical values used for recrystallisation are: intrinsic mobility M_0 ($1 \times 10^{-10}\,\mathrm{m^2\,kg^{-1}\,s}$; Nasello et al., 2005), boundary-diffusion activation energy Q ($40\,\mathrm{KJ\,mol^{-1}}$; Thorsteinsson, 2002), isotropic surface energy γ_e ($0.065\,\mathrm{J\,m^{-2}}$; Ketcham and Hobbs, 1969) and temperature was set to $T = -30\,^{\circ}\mathrm{C}$. To simulate recovery numerically, a modification of the approach proposed by Borthwick et al. (2013) was used. See Llorens et al. (2015) for a complete description of the methods.

Starting with the same initial microstructure, models with two different ratios between dynamic recrystallisation (grain boundary migration and recovery) and viscoplastic deformation were performed: 1 and 10 DRX steps per deformation (FFT) step. The time incremental for each recrystallisation step was set to $\Delta t = 6.3 \times 10^{8}\,\mathrm{s}$, giving strain rates 3.17×10^{-11} and $3.17 \times 10^{-12}\,\mathrm{s^{-1}}$ for 1 and 10 DRX step models, respectively.

3 Results

3.1 Stratigraphy and fold classification

The stratigraphic data were visually inspected for all parts of the ice core containing cloudy bands, in order to categorise disturbances of the visible layers. It has to be noted that this method is only appropriate where sufficient layers are visible, since clear ice may have been deformed as well. Figure 1 shows an overview of the layering structures we find in the NEEM ice core. All images shown are confined to the core sections above the major disturbances in the Eemian ice beginning at a depth of approximately 2200 m. Around this depth the ice is heavily sheared and the layering becomes more and more diffuse. Below that it is no longer possible to see fold structures in the visual

TCD
9, 5817–5847, 2015

stratigraphy data as the ice of the Eemian is mostly clear and heavily sheared. The panels display the scans of entire core sections of about 1.10 m, which were cut into segments of 0.55 m after scanning. The top always represents the upper part of the core segment. Some segments differ in length, as the recovered core pieces are not always exactly 1.10 m long. Some of the pieces also fractured during the recovery process or during preparation, which is highlighted with red lines in Fig. 1. The images have been partly processed by applying a Gauss filter to enhance the visibility of the layering, and therefore the grey values are no absolute measure for impurity content or of other parameters that could influence the backscatter within the ice.

The upper part of the NEEM ice core shows little or no disturbances. Figure 1a shows an example from 1430 m depth with perfectly horizontal layers. The layer thickness and opacity does vary in the core segment, and single layers have a constant thickness throughout the 10 cm wide core section. A close up of one of the layers shows no particular structure within it (Fig. 2a). Below a depth of about 1700 m the structure of the layering begins to change, as examples from depths of approximately 1760 and 1867 m show (Fig. 1b and c). Wave-like features with cm-scale amplitudes and wavelengths in the order of the core diameter can be observed. In some parts of the core segments these disturbances can be clearly followed through several layers. Figure 2b shows an enlarged section of Fig. 1b, showing a well-developed asymmetric z-fold. Its shape indicates sinistral shear and the fold is beginning to overturn. The fold hinge is a sharp feature, which can be followed over several layers. The enlargements in Fig. 2b also show that the cloudy layers themselves appear to be laminated.

For the core sections shown in Fig. 1b and c the layers vary in thickness within the core, as can be clearly seen in Fig. 2b, where the central greyish layer nearly doubles its thickness in the centre of the image due to the folding. This shape is typical for so-called similar folds in geology. Figure 1d and e show examples from 1977 and 2098 m depth, where the layering is significantly more disturbed. The vertical scale of the disturbances has risen to the scale of 10 cm (Fig. 2d and e). In between the larger-scale folds the layering appears to be more regular again, however the limited width of the core sections limits our interpretation here, as the layers could have been flattened out by shear deformation. Figure 2c shows a stack of flattened folds, where the doubling of layers is not immediately obvious to the observer when focusing the left part of the image. There are also new generations of folds standing out through their well-defined and steeper axial planes and which are not yet overturned (Fig. 2c, on the left).

At even greater depth the layering becomes less distinct (Fig. 1f–h). In some parts of these sections the layers appear to be undisturbed but inclined, which may indicate that they are part of a larger deformation structure. The now very thin layers still show new generations of folds.

3.2 Crystal fabric orientation anomalies connected to folds

In comparison to previous deep ice cores, the amount of data gathered to analyse ice fabric is relatively high. To investigate small-scale variations entire bags of 55 cm from certain depths were processed. The general evolution of ice fabric with depth in the NEEM ice core was described in Montagnat et al. (2014b). The c-axis orientation distribution develops more or less linearly from an isotropic fabric to a single maximum at a depth of about 1400 m, which represents the transition from the Holocene to the last glacial (Rasmussen et al., 2013). Within the well-developed single maximum fabric we found inclined bands of grains with a deviating c-axis orientation. We assume that the bands are planar features, but as the thin sections are vertical cuts through the cylindrical core section the inclination of the bands is not necessarily equal to the inclination of the planes. Similar bands were described in the GRIP ice core (Thorsteinsson, 1996) and the GISP2 ice core (Alley et al., 1997). In case of the NEEM ice core, however, significantly more fabric data are available, which enables us to follow these structures through entire core sections.

One of the first examples of such a band, shown in Fig. 3a, appears at a depth of 1800 m. The c-axis orientation of grains within the bands is tilted anti-clockwise relative to the single maximum, which is indicated by the blue-greenish colours in the colour wheel used to illustrate c-axis orientation (inset in Fig. 3a). The grain size does not differ from the average grain size of the sample. The subgrain boundary density in these grains does not differ significantly from the surrounding ones, which indicates that they are most likely not newly nucleated grains (Fig. 4). However, while the subgrain boundaries in grains with vertical c-axes are mostly parallel to the basal planes, they are mainly perpendicular to the basal plane in grains within the band, indicating the onset of rotation recrystallisation.

The direct comparison of the fabric data with the line scan images (Fig. 3) reveals that these bands are connected with disturbances in the layering. The inclination is in agreement with the sense of shear that is derived from the asymmetry of the folded layers. However, layer disturbances are not always visible where fabric anomalies are found.

In Fig. 5a–c the three linescan images available from the different focal depths are plotted next to each other to illustrate the three-dimensional nature of the observed folding in the layering. The shape change of the highlighted layer indicates that the fold axis shifts to the left towards the centre of the core (Fig. 5e). The thin sections for the fabric analysis are prepared from the physical properties sample in the upper part, the linescan measurement is performed on the remaining part of the core with 1 cm between the different focal planes (Fig. 5d).

Figure 6 shows an example from approx. 1978 m depth where we see finely laminated layers and asymmetric folds that indicate dextral shear. The fold hinges indicated by the arrows are not very distinct, which is probably due to light diffusion caused by the distorted fine layers. The two distinct bands in the right half of Fig. 6a are relatively steep and exhibit a small tilt in the c-axes, while the feature indicated by the central arrow is more flattened and also shows a higher tilt in the c-axes. Another example can be found in Fig. S1 of the Supplement). Where several bands occur in one core section, their inclination and orientation appears to be consistent throughout (Fig. 7).

TCD
9, 5817–5847, 2015

3.3 Model results

To understand the development of the observed fabric anomalies and the related disturbances in the layering, we simulated the fabric evolution under simple shear with an initially well developed single maximum orientation distribution. A random noise of $< 5^\circ$ was added to grain orientations. The setup of the simulation does not fully represent the probably kinematic boundary conditions in the region of the ice core where we observe the structures, which would be a combination of vertical compression and simple shear (Montagnat et al., 2014b). We, however, model these structures in simple shear for simplicity. This approach is reasonable, since there is a non-coaxial flow component in the region (NEEM Community Members, 2013). Moreover, the choice of simple-shear boundary conditions is also justified by the fact that the bands start to appear in the lower third of the ice sheet where shear stress becomes the dominant driver for deformation (Montagnat et al., 2014b).

In the model simulation vertical bands similar to the ones observed in the ice core begin to stand out after a shear strain of $\gamma = 0.6$, but start to appear already after small strains (Fig. S3). The c-axes of the grains in the bands are slightly tilted clockwise, in a synthetic sense with the imposed dextral shear. These bands intensify during the next steps and begin to tilt due to the continuing shear deformation (Fig. S2). Continuing shear causes further tilting of the c-axes orientations within the bands. The rotation of the c-axes is twice the inclination of the band, which is typical for flexural-slip kink folds (Fig. S4; Dewey, 1965; Tanner, 1989). Figure 8a–c show the c-axis orientations for the sample after shear strains of $\gamma = 1$, $\gamma = 2$ and $\gamma = 3$. The bands seem to develop in different generations, which can be distinguished by their inclination as the new bands are steeper. There are areas between the bands where orientations of c-axes rotate anti-clockwise (magenta coloured), but on a larger scale and with less well-defined boundaries. In later stages of the simulation the oldest bands begin to disintegrate with the grains recrystallizing back to a vertical c-axis fabric.

Figure 8d–f shows the development of a passive marker grid during the simulations. The blue lines were perfectly horizontal at the beginning of the simulation and can be regarded as an analogue to the stratigraphic layering observed in the ice core. It is apparent that the bands with abnormal grain orientation are connected with folding in the layering. At first these disturbances appear as small steps, but they develop into overturned folds with a short and steep limb with progressive deformation. They correspond to the well-developed bands in the fabric, and to a long, less inclined limb, representing the area in between the bands. The disturbances in the layering are permanent, and therefore the bands are visible in the passive grid even when they no longer exist in the orientation plot. The development of the kink bands is represented in the model run, but the flattening of the structures probably takes place faster under real conditions due to the additional vertical flattening caused by the overlying ice column. This may explain the existence of horizontally layered sections in the deeper parts of the NEEM ice core seen in the linescan images discussed above.

Figure 8g, h and i shows the equivalent von Mises strain-rate for the deformation steps $\gamma = 1$, $\gamma = 2$ and $\gamma = 3$. The strain-rate appears to be localized around the margins of the bands where bending strain is the highest, which is most apparent for newer bands with steep inclinations.

4 Discussion

4.1 General discussion of folds

The shape of the observed folds in the NEEM ice core is typical for similar folds, as the layers are thickened in the hinge region and thinned in the fold limbs. Similar folds are passive features, where all layers of the package are deformed in a similar way (Fig. 9a). They form by passive shearing of the layering and can evolve to become overturned z-folds or even sheath folds (Quinquis et al., 1978; Bons and Urai, 1996; Alsop and Carreras, 2007). Competence or viscosity contrast between the different

TCD
9, 5817–5847, 2015

layers plays no or only a minor role. In contrast, buckle folds (Fig. 9b) develop when layers have different viscosities. A competence contrast with a ratio of at least about 25 between strong and weak layers is required to develop distinct folds (Llorens et al., 2013a, b). When a stack of strong and weak layers is shortened, the strong layers form folds by bending, which suppresses thickening or thinning of these layers. The weak layers accommodate this bending by ductile flow into the hinge regions, a process known as flexural flow (Donath and Parker, 1964). Strong and weak layers are thus different in shape (Fig. 9b). The folding shapes observed in the NEEM core, however, appears to be consistent in a stack of several layers (Figs.1 and 2), which indicates that viscosity contrast are very low and the folds formed by passive shearing, although there may be differences in the flow strength of the ice between the layers due to different impurity content (Paterson, 1991).

Figure 10 gives an overview of the onset of folding (black line) and the evolution of an anisotropic fabric (red line) for several ice cores. Comparison with data from EDML (Faria et al., 2010) and WAIS (Fitzpatrick et al., 2014) in Antarctica and with GRIP (Thorsteinsson, 1996), GISP2 (Alley et al., 1997) and North GRIP (Svensson et al., 2005) from Greenland reveal that the onset of visible folding is dependent on the relation between vertical strain rates and shear strain rates (Fig. 10). As an approximation we can assume that in the upper two thirds of the ice column the vertical compression is dominant, while the shear component is large in the lower third (Dansgaard and Johnson, 1969; Montagnat et al., 2014b). The later onset of folding in the deeper ice cores shows that higher shear strain is required to produce visible folding due to the higher overburden pressure. If vertical compression is high, fold structures are flattened out before they overturn, and are thus no longer visible. This has been theoretically described by Waddington (2001), and is most likely the reason for the very deep onset of folding in the WAIS ice core. Another influencing factor additional to the ice thickness is the borehole location. An ice core at flanks or on divides with non-negligible flow along the ridge, samples ice which experiences more shear strain than an ice core at dome positions. While the GISP 2 and North GRIP ice cores are very similar in ice thickness to GRIP, the onset of folding for the latter is 300 m deeper, which may be due to its dome position. In the region of the NEEM ice core there is an even higher along-ridge flow. A comparison of shear strain rates profiles with depth at the NEEM, GRIP and North GRIP locations can be found in Montagnat et al. (2014b).

The EDML ice core stands out in the comparison shown in Fig. 10, as the folding begins significantly higher than the establishment of a single maximum fabric. However, Faria et al. (2010) report that a strong girdle fabric has formed in the region of the onset of folding, thus the fabric does show some anisotropy there as well.

The scale of the disturbances found in the layering of the NEEM ice core is very similar to the ones observed at EDML (Faria et al., 2010) and North GRIP (Svensson et al., 2005), for both of which a linescan dataset of comparable quality as for the NEEM ice core is available.

4.2 Kink bands as a source for folding

"Kink-bands [...] can be expected to form in any statistically homogeneous rock which has a high degree of anisotropy and which is compressed in a direction parallel to the foliation" (Cobbold et al., 1971).

Ice is a mechanically highly anisotropic mineral, as is polycrystalline ice with a strong single-maximum c-axes distribution. Kinking has been observed in single ice crystals as well as in polycrystalline aggregates under compression (Wilson et al., 1986). When compressed parallel to foliation, the initial inclination of the kink bands is 45° relative to the foliation. The ELLE model results show a similar feature: for the single maximum fabric vertical stripes develop in the first deformation stages, which only show a slight deviation of the c-axis from the vertical orientation. In a perfectly anisotropic material with slip only possible along a single plane (the basal plane in case of ice), kink folds develop where the axial plane forms the bisector of the angle between the two limbs (Fig. 9c) (Frank and Stroh, 1952; Dewey, 1965; Cobbold et al., 1971). Initial kink bands, with interlimb angles still close to 180°, thus form by geometric necessity at approximately 90° to the layering, and thus along the c-axes maximum in the lower part of ice sheets. However, kink bands are still hardly visible at this stage.

Kink bands passively rotate, if there is a layer-parallel shear component, which does not necessarily have to be the dominant deformation component. As the kink band rotates by an angle α to the long limb, the short limb has to rotate by 2α, as is observed in the NEEM core and numerical simulations (Fig. 8d–f). With progressive rotation of the kink bands they become more distinct. Rotation of the short limb occurs by sliding parallel to the basal plane with a sense opposite to the overall shearing direction (Fig. 9c). Kink bands finally "lock up" when the interlimb angle reduces to 90°, i.e. when the kink bands are approximately 45° to the layering. In the numerical simulations we see that kink bands begin to disintegrate at this stage, with recrystallization and recovery consuming the grains with deviating orientations and flow homogenizing again (see Fig. 8). However, marker lines, such as the layers in the NEEM core, will still record the kink bands, which now continue shearing and develop into passive folds.

In summary, the model results indicate that the evolution of kink bands is a consequence of a fabric with a strong anisotropy with superimposed small random disturbances. In this way grains orientated unfavourably for basal glide are rotated by rigid body rotation and internally reversed shear into a more favourable position in relation to the bulk shear strain. Thus, kinking appears to be an essential process in ice deformation under shear.

Azuma and Goto-Azuma (1996) suggested that horizontal variation in the single maximum direction could explain heterogeneous layer thinning or thickening of initially horizontal layers, eventually leading to folding. The development of kink bands is a process providing such variations in the fabric.

A difficulty in comparing the results of the simulation with the observational data is that with fabric measurements we can only capture a 2-D section of a 3-D feature. Assuming that the kink bands are planar features, the angle at which the cylinder of the ice core is cut relative to the inclination of the plane determines its appearance in the 2-D section. Thus, the inclination of the observed bands in the plane is not sufficient to describe the full orientation of the kink-band plane, but instead gives a minimum inclination of the plane. This also has to be taken into account when interpreting the fold structures on the linescan images.

Within one 55 cm section of the ice core (bag) the cutting plane through the core is consistent and so are the samples used to prepare the thin sections for the fabric measurements. Figure 7 shows that within one bag the inclinations of the kink bands are consistent as well, strengthening the assumption that they are connected to the local stress environment and to the sense of shear, projected onto the plane of the thin section or linescan image. In both examples different generations of kink bands can be detected, differing in inclination of the bands as the older bands have subject to more shear strain since their formation, and the corresponding shift in c-axes orientation, as it is seen in the model results as well.

The mechanism of kinking as a trigger for stratigraphic disturbances has already been suggested by Samyn et al. (2011). Together with the microstructural model results the observations can be interpreted with an improved understanding of the kinking process. Alley et al. (1997), who described similar bands in the GISP2 ice core, state that the observed bands are most likely not kink bands, as they would require a compressional regime in the horizontal direction. However, the model results clearly show that kink bands can form in simple shear conditions. At the moment it is not clear why the bands sometimes appear dark in the linescan images, but from deeper parts of the core where the crystals are larger in size the linescan images give indication the backscattering can be subject to the crystal orientation.

5 Summary and conclusions

The onset of small-scale folding can be observed at the start of the lower third of the NEEM ice core, which is similar to the fold evolution observed in EDML. Below a depth of about 2160 m it is no longer possible to track stratigraphic layers. The shape of the observed structures indicates that they are not buckle folds, which means that they are not originated by a competence contrast between alternating layers. The amounts of folding as well as the state of disturbance increase with depth.

Folding causes thickening of cloudy bands and can potentially influence the resolution of climate data extracted from the NEEM ice core. It also produces doubling of layers within the scale of ten centimetres below a depth of about 2100 m. In some core sections the layering appears to be intact in between larger folds in the linescan data. However, it is difficult to identify regions where the climate signal could be disturbed due to the limited diameter of the ice core.

Microstructure numerical modelling results indicate that the observed folding is initiated by kinking. The onset of kinking requires a highly anisotropic material and thus a well developed single maximum fabric. Local deviations from the single maximum in the direction of shear provide the seeds for kink band development and thus folding. Here we have shown that this process is active on the microstructural scale, but the results are in line with findings from ice flow models on the larger scale (Azuma and Goto-Azuma, 1996). The kink bands are eventually eroded through recrystallisation and recovery. Eventually the kink bands shear into passive folds that are visible in the layering, but not in the c-axes patterns.

The Supplement related to this article is available online at doi:10.5194/tcd-9-5817-2015-supplement.

Acknowledgement. This work was carried out as part of the Helmholtz Junior Research group "The effect of deformation mechanisms for ice sheet dynamics" (VH-NG-802). F. Steinbach was funded by the DFG (SPP 1158) grant BO 1776/12-1. The NEEM Linescan data as well as the NEEM fabric data has been made available by www.pangaea.de. The Authors would like to thank Sergio H. Faria and Rüdiger Kilian for helpful discussions and the editor J.-L. Tison whose suggestions helped to improve the manuscript. We also would like to thank all members of the NEEM Community who did prepare the physical properties samples in the field.

NEEM is directed and organized by the Center of Ice and Climate at the Niels Bohr Institute and US NSF, Office of Polar Programs. It is supported by funding agencies and institutions in Belgium (FNRS-CFB and FWO), Canada (NRCan/GSC), China (CAS), Denmark (FIST), France (IPEV, CNRS/INSU, CEA and ANR), Germany (AWI), Iceland (RannIs), Japan (NIPR), Korea (KOPRI), the Netherlands (NWO/ALW), Sweden (VR), Switzerland (SNF), UK (NERC) and the USA (US NSF, Office of Polar Programs).

References

Alley, R. B., Gow, A. J., Meese, D. A., Fitzpatrick, J. J., Waddington, E. D., and Bolzan, J. F.: Grain-scale processes, folding, and stratigraphic disturbance in the GISP2 ice core, J. Geophys. Res., 102, 26819–26830, 1997.

Alsop, G. I. and Carreras, J.: The structural evolution of sheath folds: a case study from Cap de Creus, J. Struct. Geol., 29, 1915–1930, doi:10.1016/j.jsg.2007.09.010, 2007.

Azuma, N. and Goto-Azuma, K.: An anisotropic flow law for ice-sheet ice and its implications, Ann. Glaciol., 23, 202–208, 1996.

Bons, P. D. and Urai, J. L.: An apparatus to experimentally model the dynamics of ductile shear zones, Tectonophysics, 256, 145–164, doi:10.1016/0040-1951(95)00161-1, 1996.

Bons, P. D., Koehn, D., and Jessell, M. W.: Lecture notes in earth sciences, in: Microdynamic Simulation, edited by: Bons, P. D., Koehn, D., and Jessell, M., Springer, Berlin, 405 pp, 2008.

Borthwick, V. E., Piazolo, S., Evans, L., Griera, A., and Bons, P. D.: What happens to deformed rocks after deformation? A refined model for recovery based on numerical simulations, J. Geol. Soc. London, 394, 215–234, doi:10.1144/SP394.11, 2013.

Cobbold, P. R., Cosgrove, J. W., and Summers, J. M.,: Development of internal structures in deformed anisotropic rocks, Tectonophysics, 12, 23–53, 1971.

Dansgaard, W. and Johnsen, S. J.: A flow model and a time scale for the ice core from Camp Century, Greenland, J. Glaciol., 8, 215–223, 1969.

Dewey, J. F.: Nature and origin of kink-bands, Tectonophysics, 1, 459–494, 1965.

Donath, F. A. and Parker, R. B.: Folds and folding, Bull. Geol. Soc. Am., 75, 45–62, doi:10.1130/0016-7606(1964)75[45:FAF]2.0.CO;2, 1964.

Faria, S. H., Freitag, J., and Kipfstuhl, S.: Polar ice structure and the integrity of ice-core paleoclimate records, Quaternary Sci. Rev., 29, 338–351, 2010.

Fitzpatrick, J. J., Voigt, D. E., Fegyveresi, J. M., Stevens, N. T., Spencer, M. K., Cole-Dai, J., Alley, R. B., Jardine, G. E., Cravens, E. D., Wilen, L. A., Fudge, T. J., and

McConnell, J. R.: Physical properties of the WAIS divide ice core, J. Glaciol., 60, 1181–1198, doi:10.3189/2014JoG14J100, 2014.
Frank, F. C. and Stroh, A. N.: On the theory of kinking. P. Phys. Soc., 65, 811–821, 1952.
Griera, A., Bons, P. D., Jessell, M. W., Lebensohn, R. A., Evans, L., and Gomez-Rivas, E.: Strain localization and porphyroclast rotation, Geology, 39, 275–278, 2011.
Griera, A., Llorens, M.-G., Gomez-Rivas, E., Bons, P. D., Jessell, M. W., Evans, L., and Lebensohn, R. A.: Numerical modeling of porphyroclast and porphyroblast rotation in anisotropic rocks, Tectonophysics, 587, 4–29, 2013.
Jessell, M. W., Siebert, E., Bons, P. D., Evans, L., and Piazolo, S.: A new type of numerical experiment on the spatial and temporal patterns of localization of deformation in a material with a coupling of grain size and rheology, Earth Planet. Sc. Lett., 239, 309–326, doi:10.1016/j.epsl.2005.03.030, 2005.
Ketcham, W. M. and Hobbs, P. V.: An experimental determination of the surface energies of ice, Philos. Mag., 19, 1161–1173, 1969.
Kipfstuhl, J.: Visual stratigraphy of the NEEM ice core with a linescanner. Alfred Wegener Institute, Helmholtz Center for Polar and Marine Research, Bremerhaven, Unpublished dataset #743062, 2010.
Lebensohn, R. A.: N-site modeling of a 3-D viscoplastic polycrystal using Fast Fourier Transform, Acta Mater., 49, 2723–2737, 2001.
Lebensohn, R. A., Montagnat, M., Mansuy, P., Duval, P., Meysonnier, J., and Phillip, A.: Modeling viscoplastic behaviour and heterogeneous intracrystalline deformation of columnar ice polycrystals, Acta Mater., 57, 1405–1415, 2008.
Llorens, M.-G., Griera, A., Bons, P. D., Roessiger, J., Lebensohn, R., and Weikusat, I.: Dynamic recrystallization of ice aggregates during co-axial viscoplastic deformation: a numerical approach, J. Glaciol., in press, 2015.
Llorens, M.-G., Bons, P. D., Griera, A., and Gomez-Rivas, E.: When do folds unfold during progressive shear?, Geology, 41, 563–566, 2013a.
Llorens, M.-G., Bons, P. D., Griera, A., Gomez-Rivas, E., and Evans, L. A.: Single layer folding in simple shear, J. Struct. Geol., 50, 209–220, 2013b.
Montagnat, M., Castelnau, O., Bons, P. D., Faria, S. H., Gagliardini, O., Gillet-Chaulet, F., Grennerat, F., Griera, A., Lebensohn, R. A., Moulinec, H., Roessiger, J., and Suquet, P.: Multiscale modeling of ice deformation behavior, J. Struct. Geol., 61, 78–108, doi:10.1016/j.jsg.2013.05.002, 2014a.

TCD
9, 5817–5847, 2015

Montagnat, M., Azuma, N., Dahl-Jensen, D., Eichler, J., Fujita, S., Gillet-Chaulet, F., Kipfstuhl, S., Samyn, D., Svensson, A., and Weikusat, I.: Fabric along the NEEM ice core, Greenland, and its comparison with GRIP and NGRIP ice cores, The Cryosphere, 8, 1129–1138, doi:10.5194/tc-8-1129-2014, 2014b.

Nasello, O. B., Di Prinzio, C. L., and Guzman, P. G.: Temperature dependence of "pure" ice grain boundary mobility, Acta Mater., 53, 4863–4869, doi:10.1016/j.actamat.2005.06.022, 2005.

NEEM Community Members: Eemian interglacial reconstructed from a Greenland folded ice core, Nature, 493, 489–494, doi:10.1038/nature11789, 2013.

Paterson, W. S. B.: Why ice-age ice is sometimes soft, Cold Reg. Sci. Technol., 20, 75–98, 1991.

Peternell, M., Russell-Head, D. S., and Wilson, C. J. L.: A technique for recording polycrystalline structure and orientation during *in situ* deformation cycles of rock analogues using an automated fabric analyser, Journal of Microscopy, 242, 181–188, doi:10.1111/j.1365-2818.2010.03456.x, 2010.

Quinquis, H., Audren, C., Brun, J. P., and Cobbold, P.: Intensive progressive shear in Ile de Groix blueschists and compatibility with subduction or obduction, Nature, 274, 43–45, 1978.

Rasmussen, S. O., Abbott, P. M., Blunier, T., Bourne, A. J., Brook, E., Buchardt, S. L., Buizert, C., Chappellaz, J., Clausen, H. B., Cook, E., Dahl-Jensen, D., Davies, S. M., Guillevic, M., Kipfstuhl, S., Laepple, T., Seierstad, I. K., Severinghaus, J. P., Steffensen, J. P., Stowasser, C., Svensson, A., Vallelonga, P., Vinther, B. M., Wilhelms, F., and Winstrup, M.: A first chronology for the North Greenland Eemian Ice Drilling (NEEM) ice core, Clim. Past, 9, 2713–2730, doi:10.5194/cp-9-2713-2013, 2013.

Roessiger, J., Bons, P. D., Griera, A., Jessell, M. W., Evans, L. Montagnat, M., Kipfstuhl, S., Faria, S. H., and Weikusat, I.: Competition between grain growth and grain size reduction in polar ice, J. Glaciol., 57, 942–948, doi:10.3189/002214311798043690, 2011.

Roessiger, J., Bons, P. D., and Faria, S. H.: Influence of bubbles on grain growth in ice, J. Struct. Geol., 61, 123–132, doi:10.1016/j.jsg.2012.11.003, 2014.

Russell-Head, D. S. and Wilson, C. J. L.: Automated fabric analyser system for quartz and ice, Geological Society of Australia, Abstracts 64, p. 159, 2001.

Samyn, D., Weikusat, I., Svensson, A., Azuma, N., Montagnat, N., and Kipfstuhl, S.: Microstructure of the NEEM deep ice core: towards quantifying stratigraphic disturbances, EGU General Assembly, Vienna, Austria, 3–8 April 2011, EGU2011-12563-1, 2011.

TCD
9, 5817–5847, 2015

Small-scale disturbances in the stratigraphy of the NEEM ice core

D. Jansen et al.

Schulson, E. M. and Duval, P.: Creep and Fracture of Ice, Cambridge University Press, Cambridge, 2009.

Svensson, A., Wedel Nielsen, S., Kipfstuhl, S., Johnsen, J., Steffensen, J. P., Bigler, M., Ruth, U., and Röthlisberger, R.: Visual Stratigraphy of the North Greenland Ice Core Project (NorthGRIP) ice core during the last glacial period, J. Geophys. Res., 110, D02108, doi:10.1029/2004JD005134, 2005.

Tanner, P. W. G.: The flexural slip mechanism, J. Struct. Geol., 11, 635–655, doi:10.1016/0191-8141(89)90001-1, 1989.

Thorsteinsson, T.: Textures and fabrics in the GRIP ice core, in relation to climate history and ice deformation (Thesis), Berichte zur Polarforschung, 205, AWI Bremerhaven, Bremerhaven, Germany, 1996.

Thorsteinsson, T.: Fabric development with nearest-neighbour interaction and dynamic recrystallization, J. Geophys. Res., 107, ECV 3-1–ECV 3-13, doi:10.1029/2001JB000244, 2002.

Thorsteinsson, T. and Waddington, E. D.: Folding in strongly anisotropic layers near ice-sheet centers, Ann. Glaciol., 35, 480–486, 2002.

Waddington, E. D, Bolzan, J. F., and Alley, R. B.: Potential for stratigraphic folding near ice-sheet centres, J. Glaciol., 47, 639–648, 2001.

Weikusat, I. and Kipfstuhl, J.: Crystal c-axes (fabric) of ice core samples collected from the NEEM ice core, Alfred Wegener Institute, Helmholtz Center for Polar and Marine Research, Bremerhaven, Unpublished dataset #744004, 2010.

Wilson, C. J. L. and Russell-Head, H. M. S.: The application of an automated fabric analyser system to the textural evolution of folded ice layers in shear zones, Ann. Glaciol., 37, 7–17, 2003.

Wilson, C. J. L., Burg, J. P., and Mitchell, J. C.: The origin of kinks in polycrystalline ice, Tectonophysics, 127, 27–48, 1986.

TCD

9, 5817–5847, 2015

Small-scale disturbances in the stratigraphy of the NEEM ice core

D. Jansen et al.

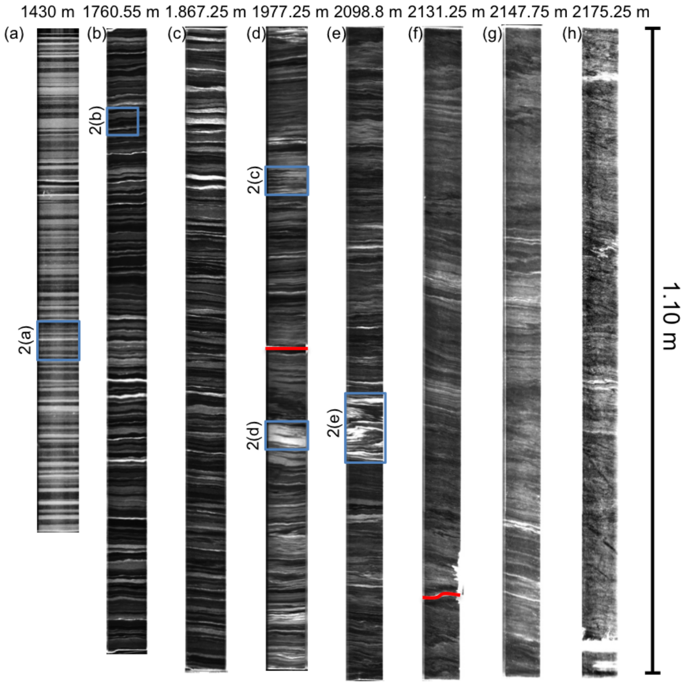

Figure 1. Visual stratigraphy overview. Linescan images of different depths. A Gauss filter was applied to images shown in panel **(a)**, **(d)**, **(e)**, **(f)**, **(g)**, and **(h)** to enhance the visibility of the layers. Red lines indicate fractures. Blue squares and associated figure codes indicate location of enlargements shown in Fig. 2. The 1.10 m line at the right indicates the scaling of the images and is also the typical length of a recovered core section.

TCD
9, 5817–5847, 2015

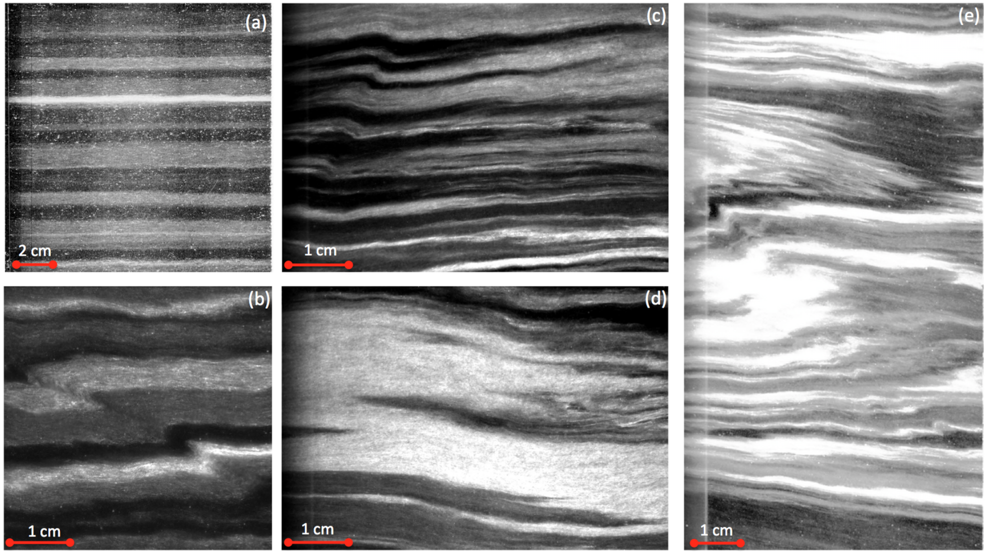

Figure 2. Close-ups from the overview Fig. 1. **(a)** Undisturbed layering. **(b)** Angular z-fold consistent throughout layering. **(c)** Different generation of folds. **(d)** Strongly disturbed layer significantly thickened. **(e)** Strongly disturbed layering with different generations of folds.

TCD
9, 5817–5847, 2015

Small-scale disturbances in the stratigraphy of the NEEM ice core

D. Jansen et al.

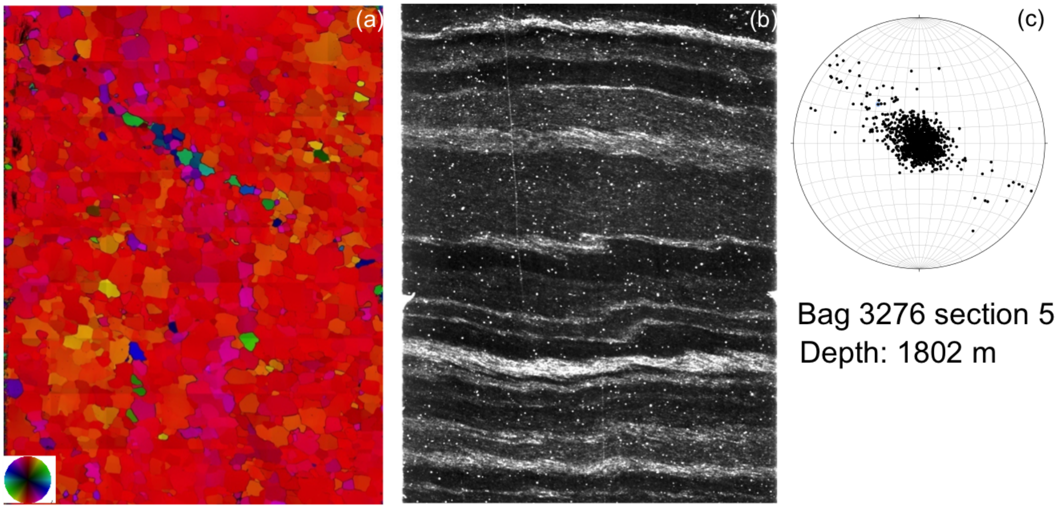

Figure 3. Comparison of fabric data and visual stratigraphy in detail, Bag 3276, approximate depth 1803 m. **(a)**'Fabric data in a vertical section, **(b)** linescan image in a vertical section, **(c)** stereoplot of c-axes orientations (horizontal plane).

TCD
9, 5817–5847, 2015

Small-scale disturbances in the stratigraphy of the NEEM ice core

D. Jansen et al.

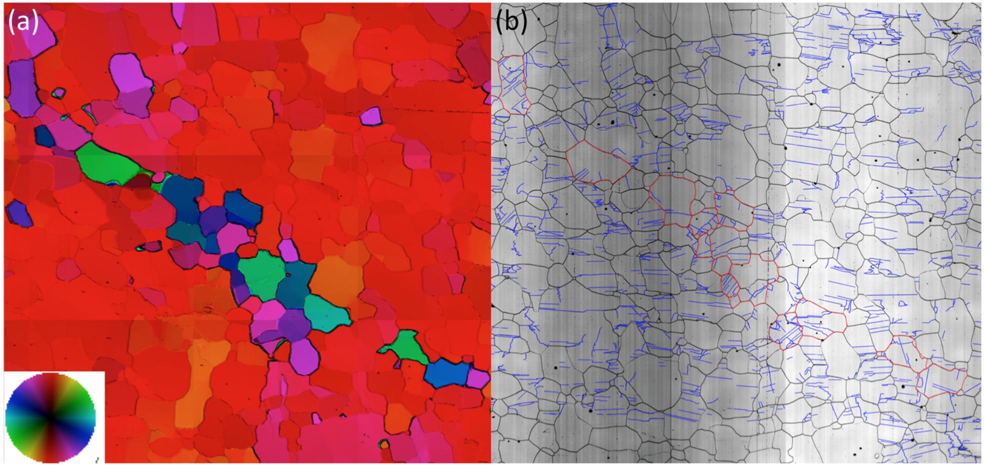

Figure 4. (a) Close-up of kink band grains at approximately 1803 m depth (bag 3276). Inset shows the colour code for c-axes orientation **(b)** subgrain structures (blue) visible on LASM (Large Area Scanning Macroscope) data. Black lines indicate grain boundaries; the red outlines highlight the kink band grains.

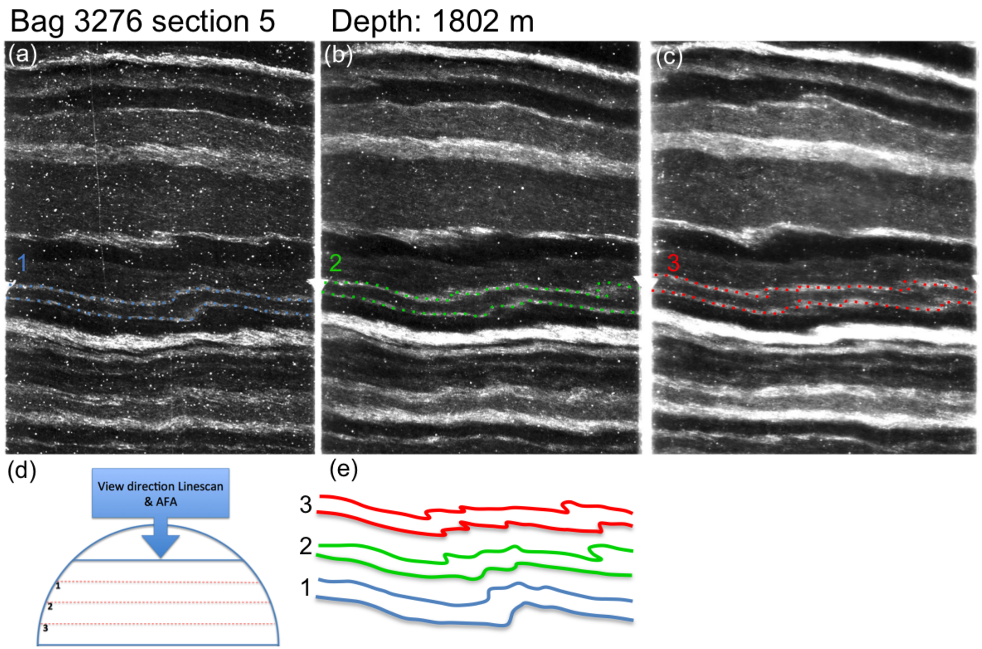

Figure 5. Linescan images from the same sample as shown in Fig. 3 from three focal depths with one highlighted layer **(a)** close to the surface, **(b)** in the centre of the core section, **(c)** close to the lower surface. **(d)** Sketch of the core sections, the upper part represents the physical properties sample, from which the thin sections are prepared. **(e)** Change of shape of the highlighted layer for the different foci.

TCD
9, 5817–5847, 2015

Small-scale disturbances in the stratigraphy of the NEEM ice core

D. Jansen et al.

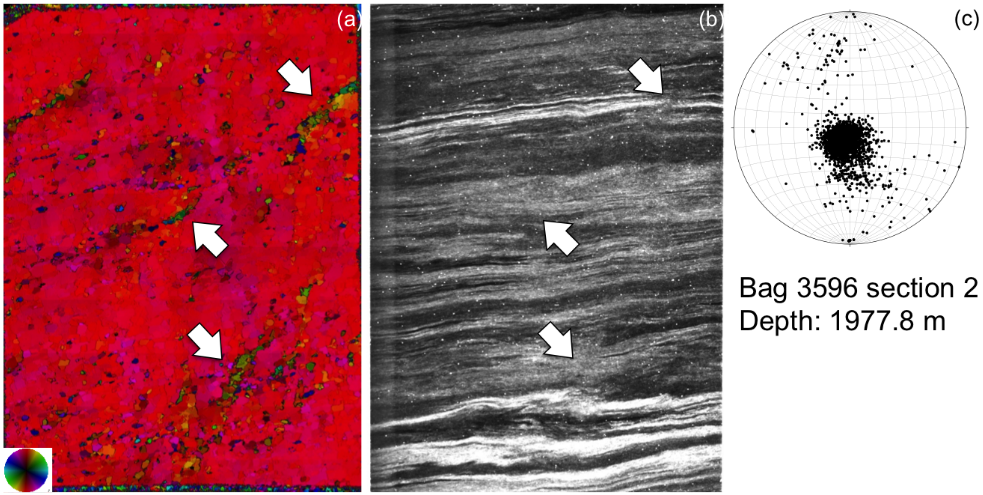

Figure 6. Comparison of fabric data and visual stratigraphy in detail, Bag 3596, approximate depth 1977.8 m. **(a)** Fabric data in a vertical section, **(b)** linescan image, in a vertical section **(c)** stereoplot of c-axes orientations (horizontal plane).

TCD
9, 5817–5847, 2015

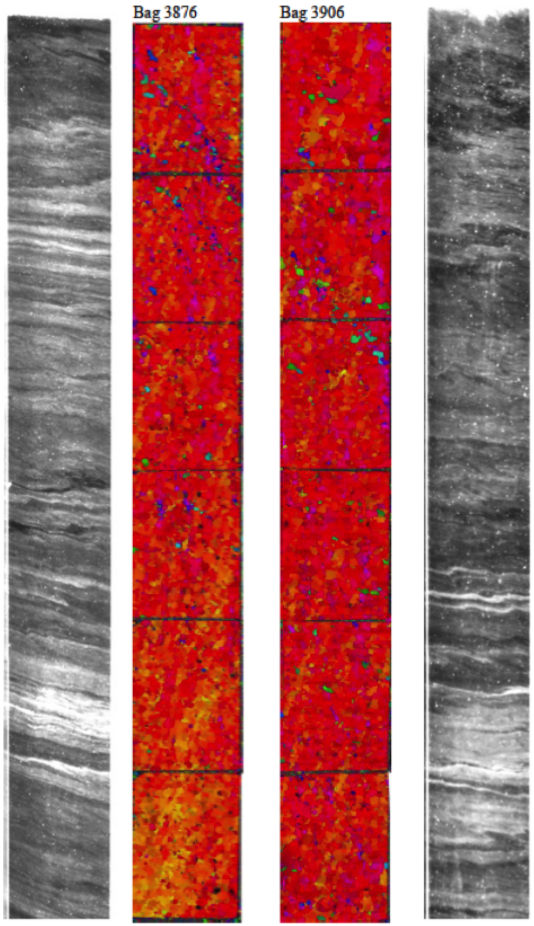

Figure 7. Comparison of entire 55 cm core sections (full bags) of linescan **(a**, **d)** and fabric data **(b**, **c)**.

TCD
9, 5817–5847, 2015

Small-scale disturbances in the stratigraphy of the NEEM ice core

D. Jansen et al.

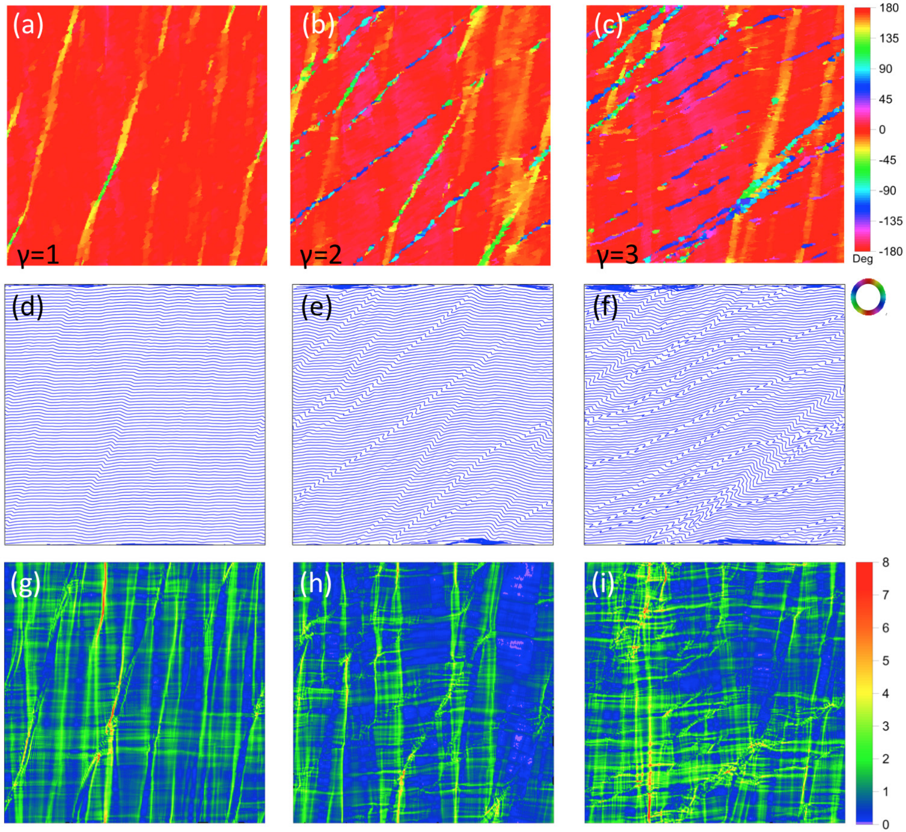

Figure 8. ELLE model results for the simple shear experiment. Panels **(a)**, **(b)** and **(c)** show c-axes orientations for shear strains of $\gamma = 1$, $\gamma = 2$ and $\gamma = 3$. Panels **(d)**, **(e)** and **(f)** show the distortion of the passive grid marker. Panels **(g)**, **(h)** and **(i)** show the equivalent von Mises strain-rate field.

TCD
9, 5817–5847, 2015

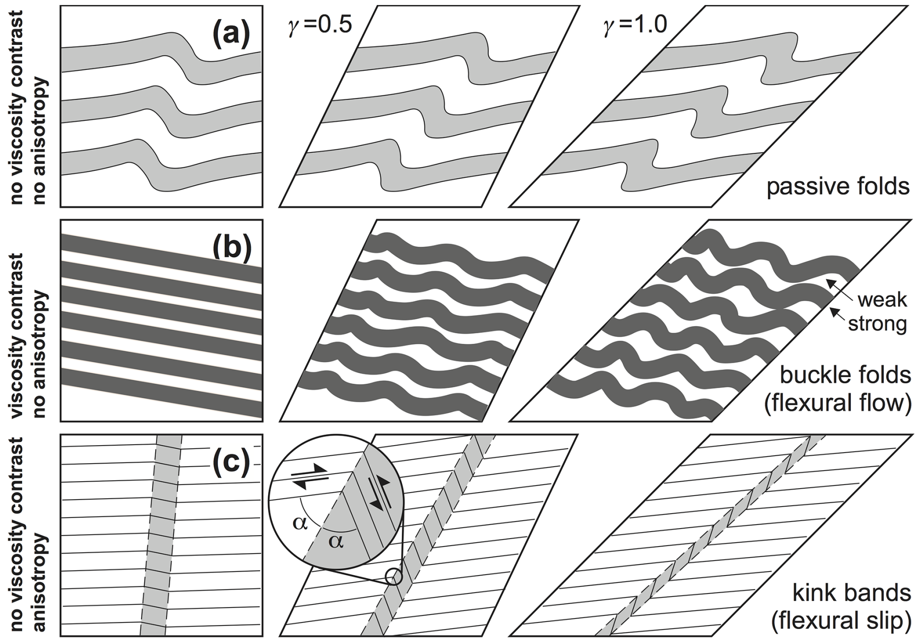

Figure 9. Basic folding mechanisms discussed in the text. **(a)** Passive folds form by shearing of disturbances in layering, without an active mechanical influence of that layering. Fold geometry is that of similar folds. **(b)** Buckle folds form by shortening of alternating strong and weak layers, in which the strong layers buckle and weak material flows into fold hinges. Fold geometry is that of parallel folds. **(c)** Kink bands form in case of strong intrinsic anisotropy, but do not require viscosity contrasts between layers.

TCD
9, 5817–5847, 2015

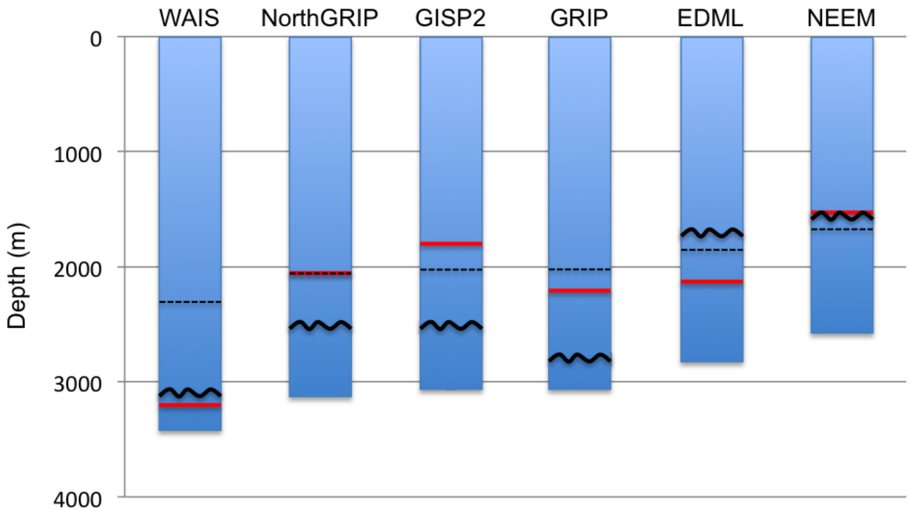

Figure 10. Comparison of the onset of visible folding in ice cores with published visual stratigraphy. The red line indicates single maximum fabric, the black line indicates onset of folding, the dashed black line indicated the lower third of the ice core. Data from Thorsteinsson (1996) (GRIP), Alley et al. (1997) (GISP2), Svensson et al. (2005) (North GRIP), Faria et al. (2010) (EDML), Fitzpatrick et al. (2014) (WAIS).

TCD
9, 5817–5847, 2015